Journal of Power Sources 245 (2014) 83–88

Contents lists available at SciVerse ScienceDirect

Journal of Power Sources

journal homepage: www.elsevier.com/locate/jpowsour

Simulation of effect of interfacial lithium flux on miscibility gap in non-equilibrium phase transformation of $LiFePO_4$ particles

N.A. Siddique [a], Ashley M. Allen [b], Partha P. Mukherjee [c,*], Fuqiang Liu [a,*]

[a] Electrochemical Energy Laboratory, Department of Materials Science and Engineering, University of Texas at Arlington, Arlington, TX 76019, USA
[b] Department of Physics, University of Texas at Arlington, Arlington, TX 76019, USA
[c] Department of Mechanical Engineering, Texas A&M University, College Station, TX 77843, USA

HIGHLIGHTS

- The effect of interfacial Li ion flux on the phase transition of $LiFePO_4$ was simulated.
- A "Mushy-Zone" model was developed to study the kinetics-induced non-equilibrium phase transition.
- Two-phase transition is found to be remarkably delayed for spherical particles.
- Growth of $LiFePO_4$ follows a well-predicted linear curve in plate-shaped particles.

ARTICLE INFO

Article history:
Received 14 May 2013
Received in revised form
12 June 2013
Accepted 13 June 2013
Available online 27 June 2013

Keywords:
Miscibility gap
Non-equilibrium
Phase transformation
Battery
Particle shape

ABSTRACT

Non-equilibrium phase transformation and effect of interfacial Li flux on miscibility gap in two-phase transformation of $LiFePO_4$ have been explored in this study. Our previously developed "Mushy-Zone" (MZ) model, accounting for sluggish Li diffusion across the two-phase interface, has been employed to study the non-equilibrium phase transformation in $LiFePO_4$ materials of Li-ion batteries. Phase transformation rate, variation of two-phase miscibility gap, and interfacial Li composition profiles have been studied for different particle shapes at varying discharge rates. Sluggish Li flux across the two-phase interface, which is believed to be the origin of the kinetically-induced non-equilibrium phase transformation, has been calculated to explain the obtained results. It is found that small particle sizes (radii of 20 nm) and slow discharge rates tend to create homogenous phase transformation (i.e., shrunk or no miscibility gap). Two-phase transformation is remarkably delayed for spherical particles at low discharge rates, leading to a lower capacity compared to that of plated-shaped particles. However, at higher discharge rates spherical particles show better capacity.

1. Introduction

Development of advanced Li ion batteries (LIBs) has become a key issue in many technological applications such as automobiles and portable electronics. To achieve a real breakthrough in the battery technology, fundamental understanding in particle-level electrochemical transport phenomena is critical.

Two-phase transition between Li-rich and Li-deficient phases within cathode materials, e.g., $LiFePO_4$, is one of the major issues that need to be focused [1]. The two-phase miscibility gap and ion transport during charge and discharge, depending on temperature [2,3], composition [4], particle size [4,5], surface coatings [6], particle shapes [7,8], and discharge rate [9], play a critical role in rate performance of LIBs. Besides, phase separation also depends on the timescale of Li insertion or extraction. Fast discharge (insertion) or charge (extraction) may lead to a kinetically-induced non-equilibrium phase transformation. Recent research also demonstrated that phase transformation in $LiFePO_4$ is strongly controlled by the strain energy induced from volume difference between the two phases [10]. Additional energy penalty due to the non-equilibrium phase transformation can further decrease the driving energy for phase transformation, resulting in a decrease of the discharge potential but increase of the charge potential [11]. Although these results demonstrate the importance of miscibility gap and non-equilibrium phase transformation, the actual mechanisms and the corresponding implications are not clear.

One of the pioneering computational models to understand the phase transformation behavior in $LiFePO_4$ was developed by

* Corresponding authors.
E-mail addresses: pmukherjee@tamu.edu (P.P. Mukherjee), fuqiang@uta.edu (F. Liu).

0378-7753/$ – see front matter © 2013 Elsevier B.V. All rights reserved.
http://dx.doi.org/10.1016/j.jpowsour.2013.06.082

Srinivasan and Newman [12] known as the core-shrinking model. One major limitation of this model is that it can only explain the battery discharge behavior at a very low rate (i.e., at equilibrium), and cannot explain the fast discharge behavior while non-equilibrium phase transformation takes place. This model was further advanced by including a moving two-phase boundary and Li ion diffusion in both phases by Wang and Kasvajjula [13]. Recently, Bazant and coworkers [14] used an electrochemical phase-field model which is based on the Cahn–Hilliard theory to study the Li intercalation inside the particles. They predicted that phase separation is suppressed above a critical current density. Delmas et al. [15] used the domino-cascade model to study the de-intercalation of $LiFePO_4$ nanoparticles and found that at any state of charge (SOC) the solid solution did not exist and instead the cathode material was a mixture of the two end members ($LiFePO_4$ and $FePO_4$).

We have developed a Mushy-Zone (MZ) model to study the kinetically-induced non-equilibrium phase transformation in $LiFePO_4$ particles [9]. The non-equilibrium miscibility gap has been shown to significantly expand and shift to higher Li compositions, leading to a reduction in two-phase solubility and battery discharge capacity. In this work, we expand our previous work and employ the MZ algorithm to investigate the non-equilibrium two-phase interface variation and transformation rate during discharge of $LiFePO_4$ particles with different shapes.

2. Model description

Transient electrochemical transport simulation was conducted on a single particle (either a plate or sphere). The transport equations for Li in different shapes of $LiFePO_4$ particles can be described as:

$$\frac{\partial c_{Li}}{\partial t} = \frac{\partial}{\partial x}\left(D_{Li}\frac{\partial c_{Li}}{\partial x}\right) \quad \text{for plate shaped particle} \tag{1}$$

$$\frac{\partial c_{Li}}{\partial t} = \frac{1}{r^2}\frac{\partial}{\partial r}\left(D_{Li}r^2\frac{\partial c_{Li}}{\partial r}\right) \quad \text{for spherical particle} \tag{2}$$

with the following boundary conditions

$$\begin{aligned} &\text{Particle center} \quad x = 0 \text{ or } r = 0 \quad j_{Li} = 0 \\ &\text{Particle surface} \quad x = l_0 \text{ or } r = r_0 \quad j_{Li} = \frac{i_n}{F} \end{aligned} \tag{3}$$

where j_{Li} is the Li flux and i_n is the intercalation current. Similar to the approach employed by Wang et al. [13,16], only 1D Li transport within a single particle (plate or sphere) is simulated. The overall Li diffusivity in one-dimension within the two-phase region can be described by Ref. [9]

$$D_{Li} = \left[(1-b)D_{Li,\alpha} + K_{Li}bD_{Li,\beta}\right]\cdot\left(\frac{1}{1-b+bK_{Li}}\right)\cdot f(c_{Li}) \tag{4}$$

where b is the volume fraction of β phase (i.e., $LiFePO_4$), $D_{Li,\alpha}$ is the Li diffusion coefficient in α phase (i.e., $FePO_4$), $D_{Li,\beta}$ is the Li diffusion coefficient in β phase, K_{Li} is the partition coefficient of Li across the miscibility gap at room temperature, and $f(c_{Li})$ is a tunable function that accounts for the interfacial diffusion ($0.00135b^{1.8}$). The two-phase interface between α and β phase is not explicitly tracked in the simulation, but rather determined by the sluggish Li diffusion and volume averaged Li concentration, i.e., $c_{Li} = (1-b)c_{Li,\alpha} + bc_{Li,\beta}$. The diffusion coefficient described by Eq. (4) applies if c_{Li} falls within the miscibility gap. The Li diffusion coefficient described in Eq. (4) avoids the discontinuity in transport properties across the narrow two-phase interface. Therefore, a coupled interplay between composition, transport, and thus phase transformation will be handled automatically through a common continuum diffusion transport simulation, based on a material balance.

Ignoring the anode overpotential and electrolyte resistance, the discharge potential E is determined from the discharge kinetics, i.e.,

$$i_n = kc_s^{0.5}\cdot(c_{max}-c_s)^{0.5}\times\left[\exp\left(\frac{0.5F}{RT}(E-E_0)\right) - \exp\left(-\frac{0.5F}{RT}(E-E_0)\right)\right] \tag{5}$$

where k is a lumped factor accounting for both the exchange current and electrolyte concentration, c_s is Li concentration at the particle surface, and F is the Faraday constant. In Eq. (5) the thermodynamic potential E_0 at the cathode particle surface is determined by the surface Li concentration c_s. Readers are referred to Ref. [9] for a complete model description and parameters used in this study.

3. Results and discussion

Our previous work has validated the MZ model against the generally-accepted core-shrinking model using performance curves and Li composition profiles at various stages of discharge [9]. In this work, we directly employ the MZ model and investigate the effect of particle size on non-equilibrium phase transformation at different rates. Discharge performance of spherical particles of $LiFePO_4$ with different radii was numerically simulated and is shown in Fig. 1. Capacities of larger $LiFePO_4$ particles (40 ad 50 nm in radius) are almost identical to those of smaller size (20 nm) at a low rate (0.5C), but significantly reduce at higher rates (1C and 2C). For example, the 20 nm $LiFePO_4$ particle delivers a capacity of 160 mAh g^{-1} almost constantly at different discharge rates; however, the 50 nm particle only shows a capacity of 100 mAh g^{-1} at a discharge rate of 2C though its capacity is around 158 mAh g^{-1} at a smaller rate of 0.5C. The reduced potential at higher discharge capacities (or reduced capacity at lower potentials) for larger particles is due to increased Li diffusion lengths. Therefore, according to Eq. (5), the potential at the $LiFePO_4$ particle surface needs to depart from the thermodynamic value (determined by Li concentration at the particle surface) further to increase the driving force and maintain the prescribed discharge current. The fluctuation in some

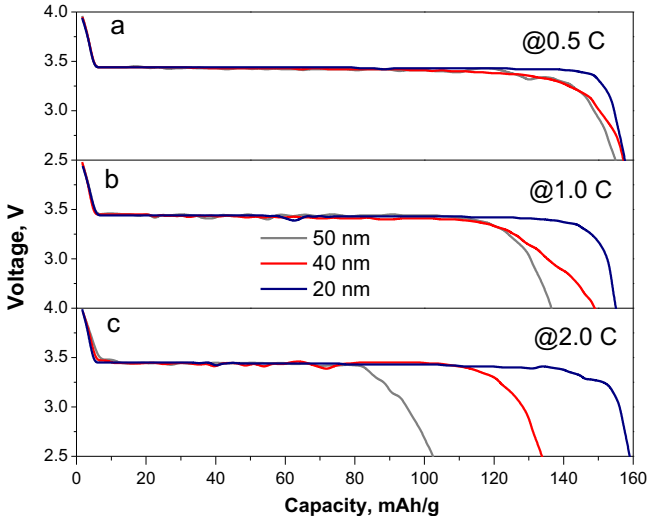

Fig. 1. Battery discharge performance of spherical particles of $LiFePO_4$ at a) 0.5C, b) 1.0C and c) 2.0C. Three different particle radii of 20, 40, and 50 nm were studied.

of the discharge curves at high discharge rates or for bigger particles is due to the fact that the discharge potential is calculated based on a single particle, where the Li compositions may vary. This compares to the experimentally-obtained discharge curves from multi-particle electrodes where the potential value is averaged over many particles. Note that only isotropic Li diffusion is assumed in the simulation; however, the conclusions in this study can be applied to lumped particles where Li transport can also be considered as isotropic.

The influence of particle size on discharge curve at different rates can be explained by different Li flux at the interface between α and β phases. Fig. 2 shows the Li flux rate at the two phase interface as a function of state of discharge (SOD, represented by x in Li_x-$FePO_4$) at 1C rate. When the two-phase front approaches the center of the particles as discharge proceeds (i.e., the SOD increases), the area of two-phase interface shrinks dramatically causing significantly higher Li flux across the interface. Simple calculation indicates that the interfacial Li flux increases linearly with particle size. This high Li flux may result in non-equilibrium phase transition which in turn gives a lower capacity. In Fig. 2 the Li flux is recalculated as a function of r/R ratio and shown in the inset. R is the size of the particle and r is the radius of the $FePO_4$ core. r/R ratio is another representation of the SOD (SOD $= 1 - (r/R)^3$); a small r/R ratio translates to a large SOD (close to the end of discharge). It is evident from Fig. 2 that for bigger particles, the Li flux at the two-phase interface is constantly higher at the same SOD and it becomes more prominent near the end of discharge.

Size of particles also impacts miscibility gap of the two phase region in a phase diagram. It is well accepted that the potential plateau in a battery discharge curve is associated with the two-phase transformation within the miscibility gap where the two phases coexist. This size dependence of the miscibility gap during discharge is shown in Fig. 3. For a fixed particle size at a constant discharge rate, the miscibility gap expands slowly at the beginning of discharge and more rapidly near the end. Also, it is evident that the miscibility gap expands more significantly for bigger particles, especially at high rates. At 0.5C, the miscibility gap remains almost constant during the entire discharge. But at higher discharge rates, an increase in particle size causes a remarkable expansion of the miscibility gap (Fig. 3c). This implies that for bigger $LiFePO_4$ particles, non-equilibrium phase transformation could likely occur during early stage of discharge.

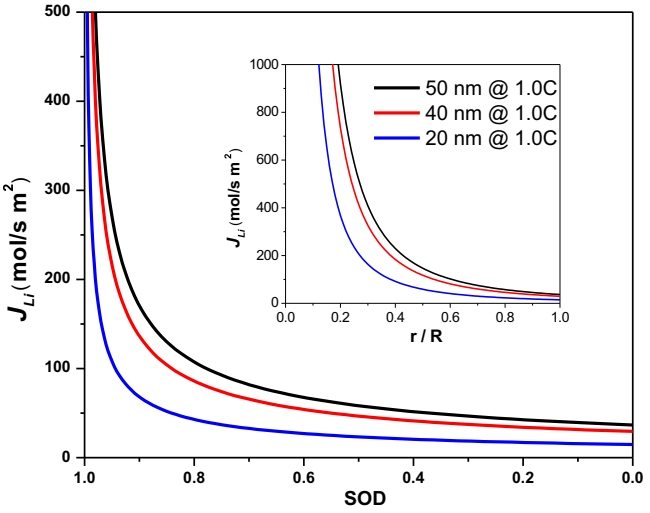

Fig. 2. Li flux at the two-phase interface as a function of state-of-discharge (SOD) for different particle sizes of $LiFePO_4$. The inset shows the interfacial Li flux at different r/R ratios.

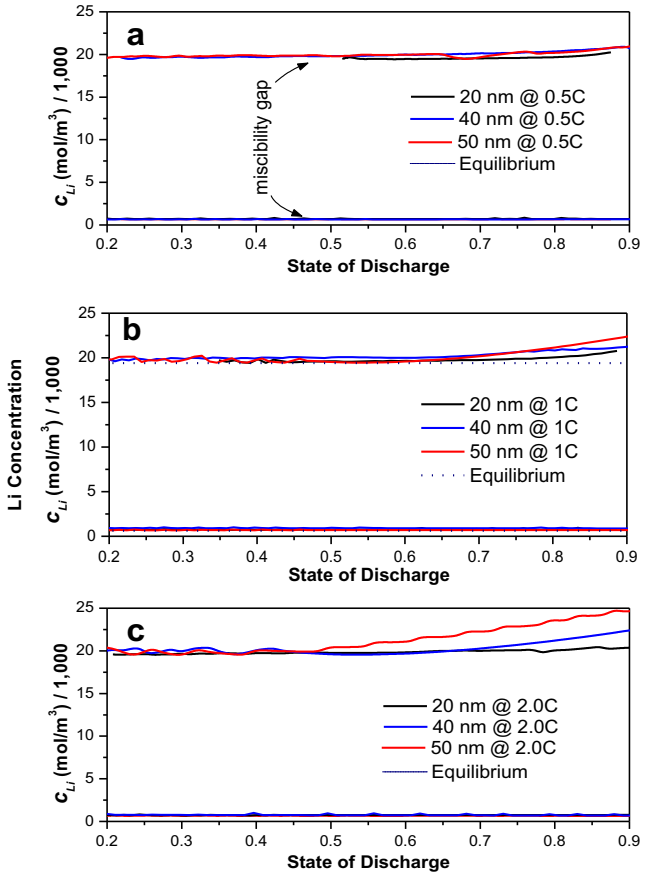

Fig. 3. Miscibility gap during the discharge process for different particle sizes at rates of a) 0.5C, b) 1C, and c) 2C.

The miscibility gap can be better understood using Li distribution profiles across the two-phase interface. At a SOD of 44%, the Li distribution profiles are shown in Fig. 4 for three different discharge rates. At lower discharge rates, the two-phase interface is wider, especially for smaller particle size, e.g., 20 nm at 0.5C. At a fixed discharge rate, bigger particles show much narrower two-phase transition. These results indicate that small particle size (20 nm) and slow discharge rate (0.5C) tend to create homogenous phase transformation (i.e., narrow or no miscibility gap). Our results are in good agreement with Meethong et al.'s experimental discovery [17] that miscibility gap contracts systematically (increased solid solution limits) with decreasing particle size.

To understand the nature of sharp two-phase interface at any stage of discharge, the gradient of chemical potential ($d\mu/dr$) for Li ion intercalation is calculated for different particle sizes. The following Cahn–Hilliard equation was used for 1D Li ion transport [18]

$$\nabla\mu_{\mathrm{Li}} = \left\{\left[-2W_c + RT\left[\frac{1}{c} + \frac{1}{(1-c)}\right]\right] \Big/ V_m + C_{1111}\cdot\Delta e_{11}^0\cdot\Delta e_{11}^0 + C_{2222}\cdot\Delta e_{22}^0\cdot\Delta e_{22}^0 + C_{3333}\cdot\Delta e_{33}^0\cdot\Delta e_{33}^0\right\}\cdot\frac{\partial c}{\partial x} + \left(2C_{1133}\cdot\Delta e_{11}^0\cdot\Delta e_{33}^0 - 2C_{1122}\cdot\Delta e_{11}^0\cdot\Delta e_{22}^0 - 2C_{2233}\cdot\Delta e_{22}^0\cdot\Delta e_{33}^0\right)\cdot\frac{\partial c}{\partial x} - \kappa\cdot\left(\frac{\partial^3 c}{\partial x^3}\right) \quad (6)$$

where V_m is the molar volume of stoichiometric $LiFePO_4$, W_c is the regular solution coefficient, C_{ijkl} is the stiffness tensor component,

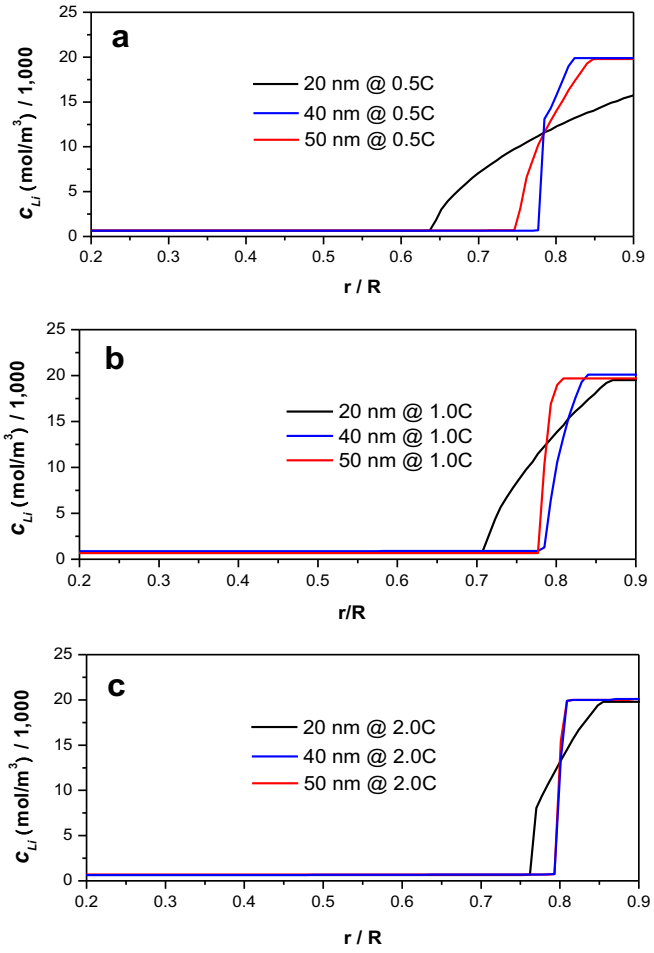

Fig. 4. Li concentration profiles at SOD of 44% for different particle size at a) 0.5C, b) 1.0C, and c) 2.0C.

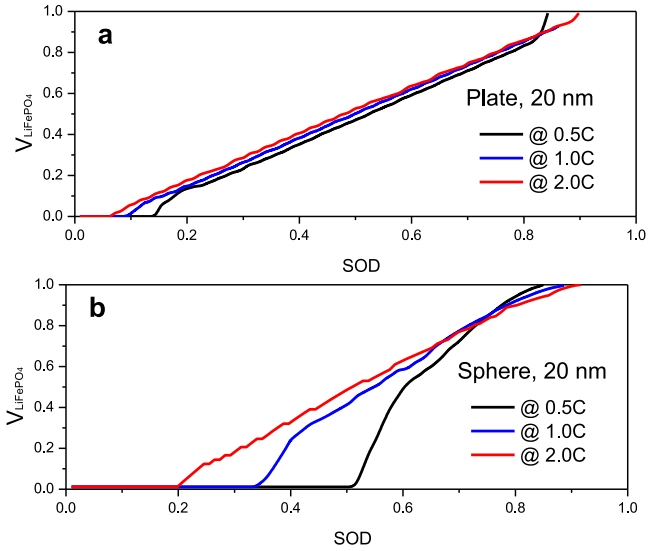

Fig. 6. Volume fraction of $LiFePO_4$ vs. SOD during discharge at different rates for a) a 20 nm-thick plate and b) a sphere with a radius of 20 nm.

$\Delta e_{ii}o$ is linear misfit between the two end members ($LiFePO_4$ and $FePO_4$), and κ is the concentration gradient coefficient. The gradient of chemical potentials for three particle sizes is plotted in Fig. 5. It is clearly observed that for bigger particle sizes the change in chemical potential is more drastic than those of smaller ones which is believed to be caused by the sharp two phase interfaces as one sees in Fig. 4. From a material point of view, the simulated Li concentration in Fig. 4 and chemical potential gradient shown in Fig. 5 are determined by the mismatch of structural properties (e.g., structure and lattice parameters) of the two phases presented in the cathode materials. Delmas et al. [15] has investigated the dynamic solubility limits in nanosized $LiFePO_4$ and concluded that coherent interfaces exist for small particles because of confinement of diffuse interface; whereas for larger particles steep interfaces could be observed since the mismatch between the two phases may be accommodated by creation of dislocations and cracks.

The Li concentration profile within a particle is directly linked to the rate of phase transformation. Fig. 6 shows the impact of particle shape on rate of phase transformation represented by volume fraction of $LiFePO_4$ as a function of SOD. The rate of phase transition surprisingly shows different trends for different particle shapes. Ideally phase transformation rate should follow the diagonals in Fig. 6. Growth of the $LiFePO_4$ phase is well predicted for plate-shaped particles though with a small lag initially; however, two-phase transformation is remarkably delayed for spherical

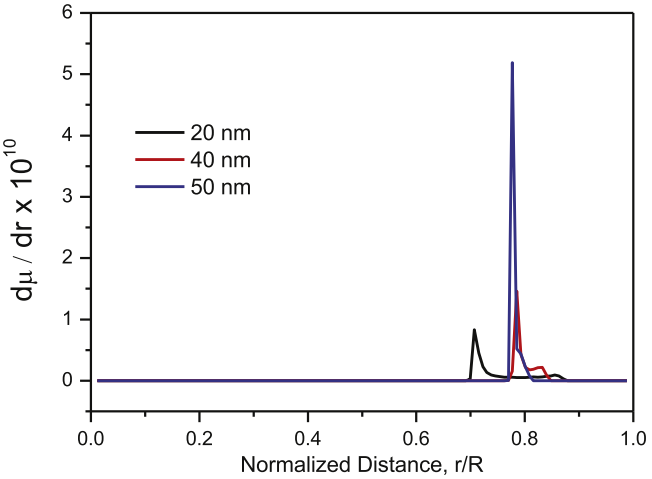

Fig. 5. Gradient of chemical potentials of spherical particles at 1C discharge rate at 44% SOD (corresponding to Fig. 4b).

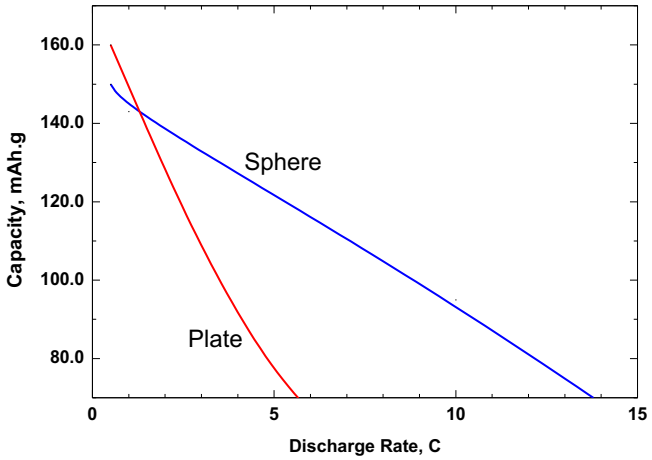

Fig. 7. Comparison of capacity as a function of discharge rate for plate-shaped and spherical particles.

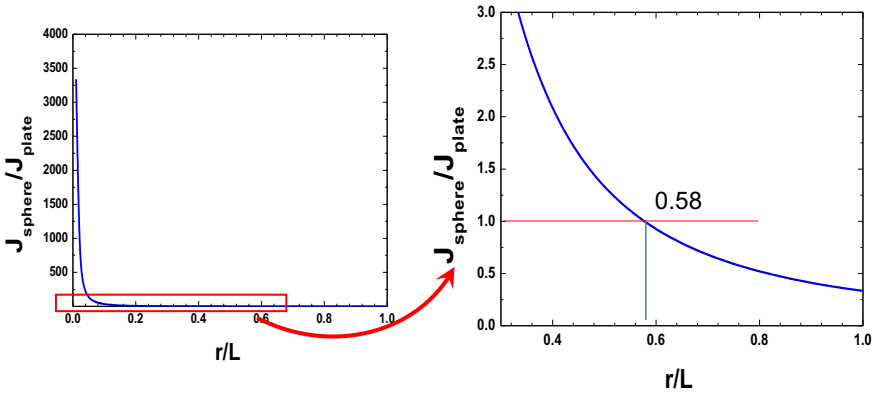

Fig. 8. Ratio of the Li ion flux at the two-phase interface for two different particle shapes during discharge.

particles, especially at low discharge rates. For example, at a discharge rate of 0.5C $LiFePO_4$ phase does not appear until $x \approx 0.5$ in Li_xFePO_4. This delay is due to increased interfacial Li flux across the two-phase boundary which could lead to non-equilibrium behavior. This delay in phase transformation has also been recently observed experimentally. Studies using in situ XRD showed the similar non-synchronized phase transition with charge/discharge plateau (i.e., phase transformation delay). Leriche et al. observed that the XRD pattern of $FePO_4$ recorded at 50% SOC did not show a theoretically equal amount of both $LiFePO_4$ and $FePO_4$ phases [19]. Chang et al. found that XRD peaks representing crystal $FePO_4$ cannot be observed until near the end of charge [20]. Quite similarly, Chiang et al. found for $LiFePO_4$ with very small particle size (34 nm) a significant phase transformation delay using XRD experiment [21]. The above results indicate that phase transformation may be more delayed or even disappear if discharge rate is further reduced. A simulation at 0.05C was done for a spherical particle (20 nm) and results showed a similarly homogeneous phase transformation path as described by Cedar et al. [22]. Despite its strong two-phase character, the phase transformation of $LiFePO_4$ can also occur through an alternative single-phase transformation path either at very low overpotential [22] or low discharge rate.

The different rate of phase transformation could lead to different discharge behavior of these particles. In our previous work [9] we studied the equilibrium and non-equilibrium phase transformation and the effect of particle shape, particularly at low discharge rates (0.5C). Here we expand the discharge rate to 15C and compare the discharge capacity of particles with different shapes. Interestingly, Fig. 7 shows that the curves of capacity as a function of discharge rate for plates and spheres cross at ca. 1.5C. At lower rates, plate-shaped particles are slightly better but show much lower capacity when discharge rate increases.

The interesting observation in Fig. 7 can be interpreted by different Li flux across the two-phase interface for different particle shapes [9]. The interfacial Li flux for plate shaped particles remains constant at a discharge rate throughout the entire discharge process, while the flux increases for spherical particles as phase transformation approaches the center of the particles. The ratio of interfacial flux between the two shapes shown in Fig. 8 indicates that at the early stage of phase transformation ($r/L > 0.58$ where r is the radius of the $FePO_4$ core and L is the plate thickness), the Li flux (required by the discharge rate) across the two-phase interface is notably smaller for spherical particles; however, as the discharge proceeds till $r/L < 0.58$ the interfacial Li flux in spheres drastically increases due to significant shrinkage of the two-phase interface, and eventually causes the kinetically-induced non-equilibrium phase transformation. As the interfacial flux spikes near the end of discharge leading to non-equilibrium phase transformation, the core of a $LiFePO_4$ sphere could not be utilized even at an extremely small rate. However, a $LiFePO_4$ plate could be completely accessed as long as the discharge rate is low enough, resulting in a higher discharge capacity. The ratio of $r/L = 0.58$ translates to a discharge capacity of $170 \times (1^3 - 0.58^3) \approx 140$ mAh g^{-1} for a $LiFePO_4$ sphere, where 170 is the theoretical capacity (in mAh g^{-1}) of $LiFePO_4$ materials. When the discharge rate increases, capacity of $LiFePO_4$ particles in both shapes decreases. However, when the discharge capacity decreases to below 140 mAh g^{-1} ($r/L = 0.58$), the lower interfacial Li flux as seen in Fig. 8 makes the sphere better utilized and therefore results in a higher capacity. This is why spherical particles show better capacity than the plates at a higher discharge rate (Fig. 7). The capacity of 140 mAh g^{-1} ($r/L = 0.58$) should therefore correspond to the point where the two curves for plate and sphere cross as shown in Fig. 7.

It is admitted that experimental validation of the simulation results on individual particle in this work is almost impossible. The conventional battery testing picks up the electrode-level phase transformation information which is thus averaged over multiple particles. Besides, in a complex multi-phase electrode structure the lithiated and delithiated phases may coexist within the same particle or as an assembly of particles [7]. Nevertheless, this study is intended to understand the non-equilibrium phase transformation in individual particle of $LiFePO_4$ and provide fundamental guidance to design high-rate battery materials from a particle-level point of view.

4. Conclusion

The effect of interfacial flux of Li on non-equilibrium phase transformation of $LiFePO_4$ particles in different shapes and discharge rates has been studied numerically. Non-equilibrium phase transformation tends to be pronounced for bigger particles even at low discharge rates. It is found that the miscibility gap expands gradually during discharge, which is evident for bigger particles, especially at high rates. Internal distribution of Li within a particle suggests that small particles (20 nm) tend to create homogenous phase transformation (i.e., no miscibility gap). Furthermore, the discharge performance is compared for plate-shaped and spherical particles. The rate of phase transformation surprisingly shows different trends for different particle shapes. Growth of $LiFePO_4$ phase follows a well-predicted linear curve in plate-shaped particles; however, two-phase transformation is remarkably delayed for spherical particles, especially at low discharge rates. The different phase transformation behavior leads to different discharge capacity at different rate: at lower rates, plate-shaped

particles are slightly better but show much lower discharge capacity when discharge rate increases; at higher discharge rates, spherical particles show better capacity.

Acknowledgments

This work was partially supported by NSF ECCS-1125588. A. Allen acknowledges supports from the LSAMP Program for Undergraduates.

References

[1] C.T. Love, A. Korovina, C.J. Patridge, K.E. Swider-Lyons, M.E. Twigg, D.E. Ramaker, Journal of the Electrochemical Society 160 (2013) A3153–A3161.
[2] M. Safari, M. Morcrette, A. Teyssot, C. Delacourt, Journal of the Electrochemical Society 156 (2009) A145–A153.
[3] A. Yamada, H. Koizumi, S.-i. Nishimura, N. Sonoyama, R. Kanno, M. Yonemura, T. Nakamura, Y. Kobayashi, Nature Materials 5 (2006) 357–360.
[4] M. Wagemaker, D.P. Singh, W.J.H. Borghols, U. Lafont, L. Haverkate, V.K. Peterson, F.M. Mulder, Journal of the American Chemical Society 133 (2011) 10222–10228.
[5] K.T. Nam, D.W. Kim, P.J. Yoo, C.Y. Chiang, N. Meethong, P.T. Hammond, Y.M. Chiang, A.M. Belcher, Science 312 (2006) 885–888.
[6] K. Zaghib, A. Mauger, F. Gendron, C.M. Julien, Chemistry of Materials 20 (2007) 462–469.
[7] M. Wagemaker, F.M. Mulder, A. Van der Ven, Advanced Materials 21 (2009) 2703–2709.
[8] K.C. Smith, P.P. Mukherjee, T.S. Fisher, Physical Chemistry Chemical Physics 14 (2012) 7040–7050.
[9] F. Liu, N.A. Siddique, P.P. Mukherjee, Electrochemical and Solid-State Letters 14 (2011) A143–A147.
[10] N. Meethong, H.Y.S. Huang, S.A. Speakman, W.C. Carter, Y.M. Chiang, Advanced Functional Materials 17 (2007) 1115–1123.
[11] Y. Zhu, C. Wang, Journal of Power Sources 196 (2011) 1442–1448.
[12] V. Srinivasan, J. Newman, Journal of the Electrochemical Society 151 (2004) A1517–A1529.
[13] U.S. Kasavajjula, C. Wang, P.E. Arce, Journal of the Electrochemical Society 155 (2008) A866–A874.
[14] P. Bai, D.A. Cogswell, M.Z. Bazant, Nano Letters 11 4890–4896.
[15] C. Delmas, M. Maccario, L. Croguennec, F. Le Cras, F. Weill, Nature Materials 7 (2008) 665–671.
[16] C. Wang, U.S. Kasavajjula, P.E. Arce, The Journal of Physical Chemistry C 111 (2007) 16656–16663.
[17] N. Meethong, H.-Y.S. Huang, W.C. Carter, Y.-M. Chiang, Electrochemical and Solid-State Letters 10 (2007) A134–A138.
[18] M. Tang, J.F. Belak, M.R. Dorr, The Journal of Physical Chemistry C 115 (2011) 4922–4926.
[19] J.B. Leriche, S. Hamelet, J. Shu, M. Morcrette, C. Masquelier, G. Ouvrard, M. Zerrouki, P. Soudan, S. Belin, E. Elkaïm, F. Baudelet, Journal of the Electrochemical Society 157 (2010) A606–A610.
[20] H.-H. Chang, C.-C. Chang, H.-C. Wu, M.-H. Yang, H.-S. Sheu, N.-L. Wu, Electrochemistry Communications 10 (2008) 335–339.
[21] N. Meethong, Y.-H. Kao, M. Tang, H.-Y. Huang, W.C. Carter, Y.-M. Chiang, Chemistry of Materials 20 (2008) 6189–6198.
[22] R. Malik, F. Zhou, G. Ceder, Nature Materials 10 (2011) 587–590.